Towards First-Principles Molecular Design of Novel Liquid Crystals-Based Chemoresponsive Systems

Luke T. Roling $^{\alpha}$, Jessica Scaranto $^{\alpha}$, Jeffrey A. Herron, Huaizhe Yu, Sangwook Choi, Nicholas L. Abbott, Manos Mavrikakis*

Department of Chemical and Biological Engineering, University of Wisconsin-Madison 1415 Engineering Drive, Madison, Wisconsin 53706-1607

 α contributed equally to this work

*corresponding author: emavrikakis@wisc.edu

Abstract

We developed a computational model to understand and predict orientational changes of surfaceanchored nematic liquid crystals (LCs) in response to chemical stimuli. In particular, we used firstprinciples calculations to study the interactions of benzonitrile (PhCN), a model for 4'-pentyl-4biphenylcarbonitrile (5CB), and dimethyl methylphosphonate (DMMP) with metal cation models
representing the substrate chemical sensing surface. We assessed the displacement of PhCN by
DMMP from their relative binding energies to ten metal cations and found a correlation between
these quantities and the experimental response time useful for predicting the response time of new
cation-LC combinations. Consideration of charge donation from chemical species in the
environment of the cations was critical for obtaining agreement between theory and experiment.
Our model is general and may be extended to the design of improved chemoresponsive LCs for
selectively detecting other chemicals of practical interest by choosing appropriate combinations of
metal cations with LCs of suitable molecular structure.

An emerging trend in materials design is the use of computational chemistry as a driver for materials discovery, with notable successes in the design of heterogeneous catalysts¹ and batteries², among others. Investigations of the anchoring of liquid crystals (LCs) to chemically functionalized surfaces and their subsequent orientational transition upon exposure to targeted analyte molecules are leading to the development and improvement of chemical and biological sensors³⁻⁸, although these innovations have required slow, laborious experiments not yet informed by computational materials discovery. In these sensors, the orientational ordering of LCs depends primarily on the chemical functionality of the surfaces used to support the LCs^{9,10}. A previous study demonstrated that the mesogen 4'-pentyl-4-biphenylcarbonitrile (5CB), which forms a nematic LC phase, can assume a parallel or tilted orientation relative to surfaces decorated with certain metal cations and a homeotropic orientation (perpendicular to the surface) relative to surfaces decorated with other cations¹¹. Homeotropic anchoring of 5CB was inferred on the basis of FTIR spectroscopy to occur through interactions of the nitrile group of 5CB with the cation. The subsequent exposure of the supported LC film to dimethyl methylphosphonate (DMMP), a common simulant of sarin nerve gas, can lead to a change in the orientation of the LC, depending on the metal cation identity. Evidence of the molecular interactions underlying the responses was obtained by using infrared spectroscopy for the cations Cu(II) and Ni(II) with 4'-octyl-4biphenylcarbonitrile (8CB) and DMMP¹². These results suggest that a more detailed understanding of the interactions between metal cations and 5CB, and the subsequent displacement of 5CB by DMMP, would provide useful fundamental information for developing a universal approach capable of predicting possible orientational transitions of LCs, which are initially anchored on surfaces containing specific metal cations, upon exposure to a specified analyte.

In this paper, we report the main results of quantum-chemical studies of the interaction of metal cations with benzonitrile (PhCN), serving as a surrogate molecule for 5CB, and DMMP. The displacement of PhCN by DMMP is predicted on the basis of the thermochemical binding energies (BEs) between each of the PhCN and DMMP molecules and the metal ion. We utilized an iterative approach in which cycles of experiments and computation created a feedback loop to unify model predictions with experimental detection properties. The results of our calculations establish a robust theoretical model for the prediction of LC responses to selected analytes of interest, and open the possibility for the accelerated design of improved chemoresponsive materials through a combined theoretical, experimental, and LC-synthetic approach.

Results and Discussion

Minimum-Energy Structures and Binding Energies

Key parameters of the energy-optimized structures of PhCN and DMMP are given in Supplementary Tables 1 and 2, Supplementary Figure 1, and the Supplementary Discussion. We observed good agreement between our computed values and previously obtained experimental ¹³ and computed ¹⁴ values.

In our first computational cycle, we calculated the binding energies of PhCN or DMMP to metal cations using the formal charge on the metal cations as determined from the metal salt precursor used in the preparation of the substrate surface (the *formal charge* approach). For example, a substrate surface created by using Cu(ClO₄)₂ as a precursor salt was modeled using a Cu²⁺ cation. The main structural parameters of the Meⁿ⁺-PhCN and Meⁿ⁺-DMMP complexes are provided in Supplementary Table 3 and the Supplementary Discussion. Representative structures

of typical Meⁿ⁺-PhCN and Meⁿ⁺-DMMP complexes are shown in Figure 1. We note that our subsequent calculations will involve cations in varying oxidation states. To avoid confusion, all cations described in this manuscript will be listed using their *formal charges* from the experimental perchlorate salt precursor (unless specifically noted otherwise).

The calculated binding energies (BE_{PhCN} and BE_{DMMP}) and final charges on the metal cations (q_f) are shown in Table 1. The differences between BE_{PhCN} and BE_{DMMP} are also provided, and are used to predict the *displacement* of 5CB by DMMP when DMMP binds more strongly by at least 0.20 eV (see Methods section). Using this model, agreement between previous experiments¹¹ and theoretical predictions of displacement was found in only one case of the ten metal cations considered (displacement of 5CB from La³⁺). Importantly, we also calculated substantial values of BE_{PhCN} for Ag⁺ (-2.21 eV) and Na⁺ (-1.41 eV), which do not exhibit homeotropic anchoring of 5CB experimentally. These significant binding energies suggest that homeotropic anchoring should occur, as they are much larger in magnitude than the threshold value adopted for weak interactions between the LC and metal cations (-0.20 eV). This suggested that our *formal charge* model is overpredicting the binding energies of liquid crystals to metal cations, which is supported by the other very large binding energies shown in Table 1.

The poor agreement between the first cycle of calculations and the experimental observations motivated the use of an alternative approach for calculating binding energies. Specifically, molecular details of the LC-substrate interface led us to hypothesize that several species (e.g. solvent, counterion) may donate electron density to the metal cation (see below for details). Accordingly, we performed a second cycle of calculations in which the charge on the metal cation was reduced from the formal charge by one unit (the *reduced charge* approach; structural results given in Supplementary Table 4). The binding energies (Table 2) calculated with

this model are substantially weaker than the formal charge values due to the reduced electron affinities of the cations in their reduced charge states. We found that all cations that bind to PhCN with a binding energy of at least -1.9 eV (*i.e.*, the strength of the reduced-charge Cd⁺ binding) exhibit homeotropic anchoring experimentally. PhCN binds more weakly to Ag^0 and Na^0 (reduced charges) than the adopted -0.20 eV threshold (as opposed to stronger than -1.0 eV using the *formal charge* approach), suggesting that only very weak interactions occur between these metals and PhCN, and as a result, the LC assumes a parallel (non-homeotropic) orientation, in agreement with experimental observations. The difference between BE_{DMMP} and BE_{PhCN} on Co^+ (reduced charge) is very small (-0.03 eV) and less negative than the cutoff value of -0.20 eV we define for displacement to occur; our prediction of no displacement on Co^+ agrees with the experimental observation. In total, we found agreement between *reduced charge* model calculations and experiment regarding displacement events in seven of the ten cases studied.

Experimental Evaluation of Response Time

These theoretical results motivated an additional cycle of experiments. The original experimental system on which this study was based¹¹ focused on whether or not the liquid crystals responded to DMMP and *not* the dynamics of those responses. Since our theoretical model predicts a magnitude of displacement energy to which dynamics might be related, we performed a new subset of experiments with an improved methodology that reduced the role of interactions other than cation-mesogen bonds in the response of the LC (see Methods for a description of differences between the old and improved experimental protocols). We used this new experimental system to explore the relationship of the calculated displacement energy and the experimentally measured response time. A sample experimental response for 5CB anchored to Al³⁺ is provided in Supplementary Figure 2.

This new cycle of experiments found that Zn²⁺ exhibited a response to DMMP, and that Cd²⁺ exhibited a weak but variable response (consistent with its small calculated displacement energy). These new experimental results agree with the computational predictions of the *reduced charge* model. Furthermore, the model predicted the highest displacement energy for Fe³⁺ (charge from metal salt precursor), and Fe³⁺ was found to exhibit the fastest response in the new experiments. In total, six cations were found to respond to DMMP exposure (increased from four, previously). As before, Ni²⁺ and Co²⁺ did not undergo a transition from homeotropic anchoring, and Ag⁺ and Na⁺ did not exhibit homeotropic anchoring. A graphical comparison of the predicted displacement energies and agreement between the calculated displacement energies (both *formal* and *reduced charge* approaches) and the new experimental cycle is shown in Figure 2. As shown in the figure, agreement between the new experiments and the *reduced charge* calculations was found in nine of ten cases; the remaining point of disagreement (Ni) corresponds to a displacement energy (-0.22 eV) very close to our cutoff value of -0.20 eV.

The response times for the cations that demonstrated an anchoring transition are plotted as an exponential function of the calculated displacement energies in Figure 3 (see Supplementary Discussion). A reasonable correlation between these quantities is found ($R^2 = 0.73$), with the exception of Cu^{2+} , which we address more fully in the next section, and Cd^{2+} , which was omitted due to its weak and variable response. This result demonstrates that the difference between BE_{DMMP} and BE_{PhCN} , despite being a purely thermodynamic quantity (no activation energy barriers for the displacement event were calculated), may be a reasonable predictor of the response time of LC films to DMMP exposure.

To evaluate the predictive capability of our model, we calculated the binding energies of three additional metal cations (*formal charges*: Sc³⁺, Cr³⁺, Fe²⁺) to PhCN and DMMP using the

reduced charge model, and measured their experimental response times. We found that all three systems responded to DMMP and their response times were predicted well by the reduced charge model binding energies to the respective metal cations (Figure 3). These results validate the predictive capability of the model, and demonstrate its utility in the future design of improved chemoresponsive materials on the basis of calculated binding energies.

Effect of Charge Transfer from Solvent

We performed additional calculations to improve our understanding of why the *reduced charge* approach leads to better agreement with experiment relative to the *formal charge approach*, choosing Cu^{2+} for further study since it was an outlier in the dataset shown in Figure 3. In the experiments, an ethanolic solution of each metal salt (in this case, Cu^{2+}) was spin-coated onto a substrate to prepare the metal surface. The solvent was then evaporated, but we postulate that: (i) some residual ethanol (EtOH) molecules might remain bound to the metal cation as a result of a possible strong interaction between the cation and EtOH in solution, and (ii) that the charge of the solvated metal cation is therefore different from its formal charge due to donation of electron density from the EtOH solvent to the cation. To test this hypothesis, we calculated the differential binding energy of EtOH and optimized cation charge resulting from the relaxation of a Cu^{2+} cation (*formal charge*) in the presence of n EtOH molecules (n = 1 - 4). These calculations showed that: (i) the cation charge decreases with increasing n, and (ii) EtOH molecules were bound progressively more weakly along with this decrease in charge as n increased (see Supplementary Discussion).

In order to further investigate this phenomenon, we computed BE_{PhCN} and BE_{DMMP} to Cu^{2+} in the presence of one and two EtOH molecules (Supplementary Discussion). We found that

calculations in the presence of two EtOH molecules particularly resembled the reduced charge model obtaining $BE_{PhCN} = -2.99$ eV and $BE_{DMMP} = -3.73$ eV. These values are within 1 eV of those calculated with the reduced charge approach (-2.56 eV, -2.81 eV), demonstrating reasonable qualitative agreement between this larger model containing Cu²⁺ bound to two EtOH molecules and the reduced charge model. Moreover, the displacement energy calculated in the complex containing two EtOH molecules (-0.74 eV) indicates that displacement of PhCN by DMMP will occur, in agreement with the reduced charge model and with the experiments. This displacement energy on Cu²⁺ calculated in the presence of two EtOH was added to Figure 3 as a hollow square. We also note that the final charge on the Cu²⁺ cation (0.68) in the presence of two EtOH resembles the (1+) charge assigned to it in the reduced charge model. We performed the same calculations with two EtOH for Zn^{2+} and Al^{3+} and found that shifts in $BE_{DMMP} - BE_{PhCN}$ also existed for these (by -0.07 eV and -0.27 eV, respectively), though these were smaller in magnitude than the shift in $BE_{\rm DMMP} - BE_{\rm PhCN}$ for ${\rm Cu}^{2+}$ (-0.49 eV), which was a particular outlier from the calculated curve in Figure 3. Two of the three explicit-solvent points (Cu²⁺ and Al³⁺) were substantially closer to the correlation established by the *reduced-charge* data points, while the Zn²⁺ value was only slightly further from the correlation; this demonstrates that our model may continue to be improved (albeit at greater computational expense) by explicit inclusion of solvent molecules in future computational cycles.

We constructed charge density difference plots, shown in Figure 4, to illustrate the effects of charge donation from EtOH molecules in the Cu^{2+} system. When using the *formal charge* approach, as in Figure 4a, significant electronic charge depletion is observed on the aromatic ring of PhCN to form the Cu-N bond. This substantial donation of electron density from PhCN to Cu^{2+} explains the exceptionally negative (i.e. strong) BE_{PhCN} calculated when using this approach. In

contrast, when using the *reduced charge* approach as shown in Figure 4b, the Cu-N bond is formed primarily by donation of electrons only from the C-N bond; minimal impact is observed on the aromatic ring's electron density, explaining the weaker binding energy when using the *reduced charge* approach.

When performing calculations using the *formal charge* on the metal cation in addition to two EtOH molecules, as shown in Figure 4c, we observe that electron density is not substantially drawn from the aromatic ring, similar to the reduced charge case. Electron density is instead donated from the EtOH molecules, in addition to the C-N bond, leading to a strong qualitative agreement with the *reduced charge* approach results (considering only the effect on the aromatic ring). We conclude that the reduced charge model, which shows good agreement with the experimental observations, represents reasonably well the interaction between the formal charge metal cations and PhCN or DMMP in the presence of two EtOH molecules, which may be more representative of the true physical environment of the metal cation. The ability to utilize the reduced charge model in place of the explicit-solvent formal charge model is important for reducing the computational cost for future calculations, due to the substantially decreased system size treated in the reduced charge model. However, we observe that the explicit inclusion of such solvent effects in future computational cycles could offer improved accuracy by fine-tuning the charge reduction on metal cations interacting with LCs and analytes; in particular, systems for which disagreement is observed between theory and experiment could be further studied by an explicit solvent model rather than a coarse-grained approximation of charge reduction by reducing by one integer unit, as we have done for Cu^{2+} .

We note briefly that this charge transfer can also be affected by the presence of other species (instead of EtOH) present in the environment of the sensing surface, including water or the

counterions in the salt precursor used to prepare the surface. We do not attempt to quantify the effects of charge transfer from other species in this work, but merely note that their effects on cation charge could be qualitatively similar to the effect of EtOH (see Supplementary Discussion).

First-Principles Design of Selective Chemoresponsive Liquid Crystals

The present computational model was developed in the context of predicting the orientational transitions of 5CB-based LCs, as represented by PhCN, upon exposure to DMMP. However, the principles behind this model are general and may be extended to guide the first-principles design of LC-based sensors for new classes of molecules/analytes. In particular, we identify three primary degrees of freedom that may be explored in future models: the identity of the analyte, the identity of the metal cation, and the molecular structure of the liquid crystal.

First, the choice of analyte is not limited to DMMP, but could in principle include any molecule binding to metal cations with sufficient strength to displace a LC. The selection of analytes will be dictated by demand for highly sensitive and selective detection in a range of applications, including (but not limited to) medical, security, and generic industrial safety applications.

Second, as illustrated in this study, the choice of metal cation strongly influences the detection capabilities of these LCs. The metal cations explored computationally thus far only represent a subset of those available for experimental applications. By performing calculations on a greater set of metal cations in a range of commercially-available oxidation states, computational screening can identify combinations of LCs and metal cations with improved sensitivity toward detection of specific analytes of interest. In particular, computations will seek to identify metal

cations that bind particularly strongly to an analyte of interest, so that the analyte might displace a weaker-binding LC from the metal cation binding site.

Third, the methods described in this study may be applied to the *selective* detection of chemical analytes by comparing their relative binding energies to individual metal cations (in addition to the binding energy of the LC to the metal cation). To briefly explore this possibility, we note that water (in the form of ambient humidity) is ubiquitous in many sensor applications and presents the possibility for "false-alarm" detection of a LC-based sensor. We evaluated the binding energies of water to all the metal cations considered in this study (Supplementary Table 5). For those cations exhibiting homeotropic anchoring experimentally (i.e. excluding Na⁰ and Ag⁰), we found that water binds much more weakly than PhCN (by at least 0.45 eV) and DMMP (by at least 0.80 eV). This suggests that water should not displace PhCN and would be noncompetitive with DMMP detection. We performed an additional set of detection experiments by exposing supported films of 5CB to ambient humidity (Supplementary Figure 4), which showed that the liquid crystal orientation was indeed unaffected by the presence of ambient humidity upon extended exposure for one hour. The possibility of selective detection suggests the future design of systems with liquid crystals and metal cations specifically chosen to yield a fast, selective response to a targeted chemical.

Fourth, the binding properties of the LCs themselves can be adjusted through modification of the functional groups through which they bind to the metal cations, as well as general modification of their detailed larger molecular structure. In particular, replacement of the nitrile termination in 5CB/PhCN with other functional groups can tailor the LC-metal cation interaction to the optimal strength for specific analyte detection. Ideal LCs will bind to metal cations more weakly than the 5CB/PhCN studied in this work, so that displacement of the liquid crystal will be

more favorable thermodynamically. However, LCs must still bind sufficiently strongly to enable homeotropic anchoring to the metal cations, so binding energy optimization must be carefully considered. Quantum chemical calculations can definitely inform and guide the organic synthesis of the respective promising LC molecules.

Finally, our calculations have shown that the exact method of synthesizing specific chemoresponsive materials, including solvents used in the synthetic protocol, might be selectively adjusted to fine-tune the effective charge on the metal cation, thereby providing a useful secondary degree of freedom worth considering in future design of LC-based sensors.

Conclusion

We successfully developed a first-principles approach to predict the displacement of 5CB, represented by benzonitrile (PhCN), by dimethyl methylphosphonate (DMMP) on the basis of calculated thermochemical binding energies utilizing integrated cycles of theory and experiment. We found that decreasing the initial metal cation charge by one unit relative to that in the metal salt used to anchor the LC molecules leads to a better prediction of LC displacement by DMMP. The better performance achieved by decreasing the initial charge of the metal cations was rationalized by the effect of electronic charge transfer from residual EtOH solvent used in the experimental preparation of the surfaces exposing the metal cations. Moreover, we elucidated a correlation between the predicted displacement energy of DMMP by PhCN and the experimentally measured orientational response time of 5CB to DMMP that can be used to predict the response time of new chemoresponsive systems. Our calculations additionally predict that the response should be selective with respect to water, as water binds much more weakly than do both DMMP and PhCN, which explains the lack of experimental response of the supported LC to ambient

humidity. Finally, although this model was developed in the context of DMMP detection by 5CB, the principles and methods established in this study are general and can be applied for developing sensors for the selective detection of a broad range of analytes by a variety of liquid crystals, thereby opening new opportunities towards a molecular-level design of novel sensors based on first-principles methods.

Acknowledgments

We thank John Cayton for his contributions to the calculations and Dr. Tibor Szilvási for his comments on the manuscript. This work was supported by the National Science Foundation (DMREF grant DMR-1435195) and the Army Research Office (W911NF-14-C-0165). The Shared Experimental Facilities of the Wisconsin MRSEC were used in this study (DMR-1121288). Calculations were performed at supercomputing centers located at EMSL, which is sponsored by the DOE Office of Biological and Environmental Research at PNNL; CNM at ANL, supported by DOE contract DE-AC02-06CH11357; and NERSC, supported by DOE contract DE-AC02-05CH11231.

Contributions

L. T. R., J. S., and J. A. H. performed the modeling and analysis, which were supervised by M. M., and all of them contributed to the preparation of the manuscript. H. Y. and S. C. performed the experiments, which were supervised by N. L. A., and all of them contributed to the preparation of the manuscript.

Competing financial interests

The authors declare no competing financial interests.

Corresponding author

References

- Norskov, J. K., Bligaard, T., Rossmeisl, J. & Christensen, C. H. Towards the computational design of solid catalysts. *Nature Chemistry* **1**, 37-46 (2009).
- 2 Kang, K. S., Meng, Y. S., Breger, J., Grey, C. P. & Ceder, G. Electrodes with high power and high capacity for rechargeable lithium batteries. *Science* **311**, 977-980 (2006).
- Gupta, V. K., Skaife, J. J., Dubrovsky, T. B. & Abbott, N. L. Optical amplification of ligand-receptor binding using liquid crystals. *Science* **279**, 2077-2080 (1998).
- Zou, Y., Namkung, J., Lin, Y. B., Ke, D. & Lindquist, R. G. Influence of a bias voltage on surface-driven orientational transitions for liquid crystal-based chemical and biological sensors. *J. Phys. D Appl. Phys.* **44** (2011).
- Zou, Y., Namkung, J., Lin, Y. B. & Lindquist, R. Optical monitoring of anchoring change in vertically aligned thin liquid crystal film for chemical and biological sensor. *Appl. Optics* **49**, 1865-1869 (2010).
- 6 Shah, R. R. & Abbott, N. L. Principles for measurement of chemical exposure based on recognition-driven anchoring transitions in liquid crystals. *Science* **293**, 1296-1299 (2001).
- Zhong, S. & Jang, C. H. Nematic liquid crystal micro-droplets on solid surfaces and their ordering transition in bulk aqueous solution. *Liquid Crystals* **42**, 1436-1443 (2015).
- 8 Liu, Y. Y. & Yang, K. L. Applications of metal ions and liquid crystals for multiplex detection of DNA. *Journal of Colloid and Interface Science* **439**, 149-153 (2015).
- 9 Jerome, B. Surface Effects and Anchoring in Liquid-Crystals. *Rep. Prog. Phys.* **54**, 391-451 (1991).
- Cognard, J. Alignment of Nematic Liquid-Crystals and Their Mixtures. *Mol. Cryst. Liq. Cryst.*, 1-77 (1982).
- Yang, K. L., Cadwell, K. & Abbott, N. L. Mechanistic study of the anchoring behavior of liquid crystals supported on metal salts and their orientational responses to dimethyl methylphosphonate. *J. Phys. Chem. B* **108**, 20180-20186 (2004).
- 12 Cadwell, K. D., Alf, M. E. & Abbott, N. L. Infrared spectroscopy of competitive interactions between liquid crystals, metal salts, and dimethyl methylphosphonate at surfaces. *J. Phys. Chem. B* **110**, 26081-26088 (2006).
- Hellwege, K. H. A. M. Landolt-Bornstein: Group II: Atomic and Molecular Physics Volume 7: Structure Data of Free Polyatomic Molecules. (Springer-Verlag, 1976).
- 14 Yang, L., Shroll, R. M., Zhang, J. X., Lourderaj, U. & Hase, W. L. Theoretical Investigation of Mechanisms for the Gas-Phase Unimolecular Decomposition of DMMP. *J. Phys. Chem. A* **113**, 13762-13771 (2009).
- 15 Gaussian 09, Revision A.02 (Gaussian, Inc., Wallingford, CT, 2009).
- Montgomery, J. A., Frisch, M. J., Ochterski, J. W. & Petersson, G. A. A complete basis set model chemistry. VII. Use of the minimum population localization method. *J. Chem. Phys.* **112**, 6532-6542 (2000).
- Montgomery, J. A., Frisch, M. J., Ochterski, J. W. & Petersson, G. A. A complete basis set model chemistry. VI. Use of density functional geometries and frequencies. *J. Chem. Phys.* **110**, 2822-2827 (1999).
- Becke, A. D. Density-Functional Thermochemistry .3. The Role of Exact Exchange. *J. Chem. Phys.* **98**, 5648-5652 (1993).

- 19 Stevens, W. J., Krauss, M., Basch, H. & Jasien, P. G. Relativistic Compact Effective Potentials and Efficient, Shared-Exponent Basis-Sets for the 3rd-Row, 4th-Row, and 5th-Row Atoms. *Can. J. Chem.* **70**, 612-630 (1992).
- Cundari, T. R. & Stevens, W. J. Effective Core Potential Methods for the Lanthanides. *J. Chem. Phys.* **98**, 5555-5565 (1993).
- Boys, S. F. & Bernardi, F. Calculation of small molecular interactions by differences of separate total energies some procedures with reduced errors. *Mol. Phys.* **19**, 553-& (1970).
- Simon, S., Duran, M. & Dannenberg, J. J. How does basis set superposition error change the potential surfaces for hydrogen bonded dimers? *J. Chem. Phys.* **105**, 11024-11031 (1996).
- Mulliken, R. S. Electronic population analysis on LCAO-MO molecular wave functions. I. *J. Chem. Phys.* **23**, 1833-1840 (1955).
- 24 Hunter, J. T., Pal, S. K. & Abbott, N. L. Adsorbate-Induced Ordering Transitions of Nematic Liquid Crystals on Surfaces Decorated with Aluminum Perchlorate Salts. *ACS Appl. Mat. & Inf.* **2**, 1857-1865 (2010).

Methods

Computational

We initially considered periodic slab models to describe the interactions between the metal cations and PhCN/DMMP. In particular, we attempted planewave DFT calculations on extended surfaces of pure metals (e.g. (111) or (100) facets of fcc metals), but found poor agreement between these models and experimental results. We also considered models in which the metal ions were charged. We finally considered surface models of bulk metal perchlorate salts, but found that these models were too complicated due to the varying stoichiometry and crystal structures, along with the very high computational costs associated with such models, rendering them impractical for our modeling purposes. We therefore developed the simple, straightforward modeling approach described in the following sections, in which the surface is replaced by an appropriately charged metal cation.

Calculations were performed with *Gaussian 09*¹⁵ using the CBS-QB3 Complete Basis Set method, a highly accurate composite method available for atomic numbers up to 36^{16,17}. In the CBS-QB3 method, the energy-optimized structures and the zero-point energy (ZPE) were computed at the B3LYP/CBSB7 level of theory. Calculations involving metals with atomic number higher than 36 (i.e. La, Cd, and Ag), for which the CBS-QB3 method was not available, were performed at the B3LYP level¹⁸ using the compact effective potentials CEP-121G basis set^{19,20}. The Counterpoise method^{21,22} was used to correct the BEs for the basis set superposition error (BSSE) for those metals computed at the B3LYP/CEP-121G level of theory.

The binding energies of PhCN and DMMP (BE_{PhCN} and BE_{DMMP}) to metal cations were calculated as the difference between the total energy of the complex of the metal and the molecule ($E_{complex}$) and the sum of the total energies of the isolated Me^{n+} (E_{Me}) and the isolated molecule ($E_{molecule}$):

$$BE = E_{\text{complex}} - E_{\text{Me}} - E_{\text{molecule}}$$

A negative (positive) value of *BE* indicates that the formation of the complex between the metal cation and the molecule is a thermodynamically favorable (unfavorable) process.

Our energy optimization calculations for the Meⁿ⁺-PhCN and Meⁿ⁺-DMMP complexes consider only binding of the metal cations to the N atom of the nitrile group (for PhCN) or the phosphoryl O atom (for DMMP). This treatment is consistent with FTIR spectroscopy that identified these as the primary functional groups through which binding occurs^{11,12}. Binding of metal cations to other functional groups/atoms on those molecules was briefly investigated and found to be much weaker, and is therefore neglected in the following analyses.

Considering the accuracies of both adopted methods (CBS and B3LYP), which are typically accurate for calculating absolute quantities (in this case, binding energies) to within 0.1-0.2 eV, and after comparing our model predictions with available experimental data, we assume that displacement of PhCN by DMMP will take place when, for a particular metal cation, BE_{DMMP} is at least 0.20 eV stronger (more negative) than the BE_{LC} , that is: $BE_{DMMP} - BE_{PhCN} < -0.20$ eV. We expect no displacement to take place if this difference is more positive than -0.20 eV. In this sense, the cutoff energy is a parameter that accounts for the uncertainty associated with the calculated binding energies as well as additional sources of error arising from complex environmental phenomena not considered by the model. For example, a gas-phase reference state of isolated molecules is not physically representative of the liquid-phase environment of these molecules; relatively weak intermolecular interactions (relative to binding of 5CB/DMMP to the metal cation) such as those between 5CB molecules and between DMMP and 5CB are implicitly accounted for in this cutoff parameter. Entropic corrections to the free energy of displacement are also not explicitly accounted for, and represent an additional source of error.

Furthermore, in order for homeotropic anchoring to occur, we require a certain (negative) binding energy between the metal cation and the PhCN molecule. In particular, again considering the typical computational accuracy and the effects of other factors neglected by this model (in particular, entropy of adsorption and self-interaction between 5CB molecules in the liquid state), we suggest that the BE_{PhCN} must be stronger than (more negative than) -0.20 eV for homeotropic anchoring; no interaction occurs for weaker (more positive) BE values, which would correspond to a parallel orientation of the LC relative to the salt substrate surface. We adopt this cutoff value as a model parameter in the absence of an additional set of experiments to rigorously determine the threshold value of BE_{PhCN} required for homeotropic anchoring, which should lie between the

smallest computed value for which anchoring is observed (-1.91 eV for Cd⁺) and the largest computed value for which anchoring does not occur (-0.19 eV for Na⁰). We finally note that these threshold values were selected in the context of displacement of 5CB by DMMP. Future experiments may be able to better identify a more precise value of the cutoff energy not only for this system, but also for systems utilizing new liquid crystal molecules with modified functionalities that may have dramatically different entropic corrections to the free energy or self-interaction properties than those found in liquid 5CB.

The value of the final charge (after energy minimization of the complex) on the metal atom (q_f) in its interaction with analytes or LCs was obtained through Mulliken population analysis²³.

Experimental

Experiments were conducted according to the procedure established in our recent work²⁴, which demonstrated that the loading of metal salt deposited on the surface can affect the orientational change of anchored LCs. We note that early studies¹¹ used high metal salt loadings that oriented LCs through both LC-cation interactions as well as other intermolecular interactions (e.g. through creation of an electrical double layer). The methodology adopted in the present work used metal salt loading that oriented the LCs largely through LC-cation bonds, which is in closer agreement with the adopted computational model.

Metal ions were deposited on the bottom surface of polymeric microwells (200 μm diameter, 5 μm depth) by spincoating 10 mM ethanolic solutions of metal perchlorates at 3000 rpm for 30 s (spincoater from Laurell Technologies, PA). Next, the microwells were filled with 5CB using a micropipette. The microwells were then exposed to a stream of N₂ containing DMMP (10 ppm) within a flow cell with glass windows, allowing observation of the optical image of 5CB

through a polarized optical microscope. The flow of gas containing DMMP was controlled to 300 ml/min by a rotameter (Aalborg Instruments and Control, Orangeburg, NY). The optical image of the LC was recorded using an Olympus camera (Olympus C2040Zoom, Melville, NY) and WinTV software (Hauppauge, NY). For experiments involving water vapor (i.e. no DMMP), microwells were synthesized according to the above procedure and were then exposed to open air in the lab for one hour. The room temperature was 26°C and the relative humidity was 31% (corresponding to a water vapor concentration around 10,000 ppm).

Table 1: Binding energy [eV] and final metal charge (q_f) for the minimum energy structures of Meⁿ⁺–PhCN and Meⁿ⁺–DMMP using the *formal charge* approach. Agreement regarding displacement events between theory and the original experiments was only seen in one of ten cases. After the follow-up experiments, agreement regarding displacement increased to three of ten cases (due to displacement of 5CB from Cd and Zn in the follow-up experiments).

Me ⁿ⁺	$BE_{ m PhCN}$	q_f	BE_{DMMP}	q_f	BE_{DMMP}	Disp.	Disp.	Agreement ^c
					- BE _{PhCN}	(Calc) ^a	(Exp) ^b	
A1 ³⁺	-24.69	1.03	-19.82	1.74	4.87	No	Yes	No
Fe^{3+}	-20.31	1.60	-19.63	1.51	0.68	No	Yes	No
La^{3+}	-8.56	2.32	-10.15	2.35	-1.59	Yes	Yes	Yes
Cd^{2+}	-6.49	1.22	-7.33	1.39	-0.84	Yes	No	No
Co^{2+}	-6.88	0.87	-7.72	1.22	-0.84	Yes	No	No
Cu^{2+}	-9.88	0.81	-8.52	1.31	1.36	No	Yes	No
Ni^{2+}	-7.66	0.86	-8.26	1.23	-0.60	Yes	No	No
Zn^{2+}	-6.81	1.34	-8.17	1.27	-1.36	Yes	No	No
Ag^+	-2.21	0.73	-2.27	0.79	-0.06	No	No Bind	No
Na ⁺	-1.41	0.83	-1.71	0.89	-0.30	Yes	No Bind	No

^a: Computed displacement of PhCN by DMMP. ^b: Experimental displacement of PhCN by DMMP, from previous studies¹¹. ^c: Agreement between computed and experimental displacement. "No Bind" indicates no homeotropic anchoring of the liquid crystal to the metal cation. Displacement is assumed to occur when $BE_{DMMP} - BE_{PhCN} < -0.20$ eV.

Table 2: Binding energy [eV] and final metal charge (qf) for the minimum energy structures of Meⁿ⁺-PhCN and Meⁿ⁺-DMMP using the *reduced charge* approach. Agreement regarding displacement events between theory and experiment was initially seen in seven of ten cases, as shown below. After the follow-up experiments, agreement regarding displacement increased to nine of ten cases (due to displacement of 5CB from Cd and Zn in the follow-up experiments). Further, the disagreement in the Ni case arises from only a very small difference (0.02 eV) between the displacement energy and the adopted energy threshold for the displacement event.

Me ⁽ⁿ⁻¹⁾⁺	$BE_{ m PhCN}$	q_f	BE_{DMMP}	q_f	$BE_{\rm DMMP}$	Disp.	Disp.	Agreement ^c
					- BE _{PhCN}	(Calc) ^a	(Exp) ^b	
Al^{2+}	-7.45	1.36	-8.60	1.36	-1.15	Yes	Yes	Yes
Fe^{2+}	-5.70	1.58	-8.08	1.37	-2.38	Yes	Yes	Yes
La^{2+}	-4.06	1.77	-5.20	1.64	-1.14	Yes	Yes	Yes
Cd^+	-1.91	0.74	-2.27	0.77	-0.36	Yes	No	No
Co^+	-2.51	0.83	-2.54	0.61	-0.03	No	No	Yes
Cu^+	-2.56	0.77	-2.81	0.70	-0.25	Yes	Yes	Yes
Ni^+	-2.56	0.77	-2.78	0.67	-0.22	Yes	No	No
Zn^+	-2.23	0.64	-2.79	0.67	-0.56	Yes	No	No
Ag^0	-0.08	-0.05	-0.17	-0.04	-0.09	No Bind	No Bind	Yes
Na ⁰	-0.19	-0.13	-0.44	-0.14	-0.25	No Bind	No Bind	Yes

^a: Computed displacement of PhCN by DMMP. ^b: Experimental displacement of PhCN by DMMP, from previous studies¹¹. ^c: Agreement between computed and experimental displacement. "No Bind" indicates no homeotropic anchoring of the liquid crystal to the metal cation. Displacement is assumed to occur when BE_{DMMP} - BE_{PhCN} < -0.20 eV.

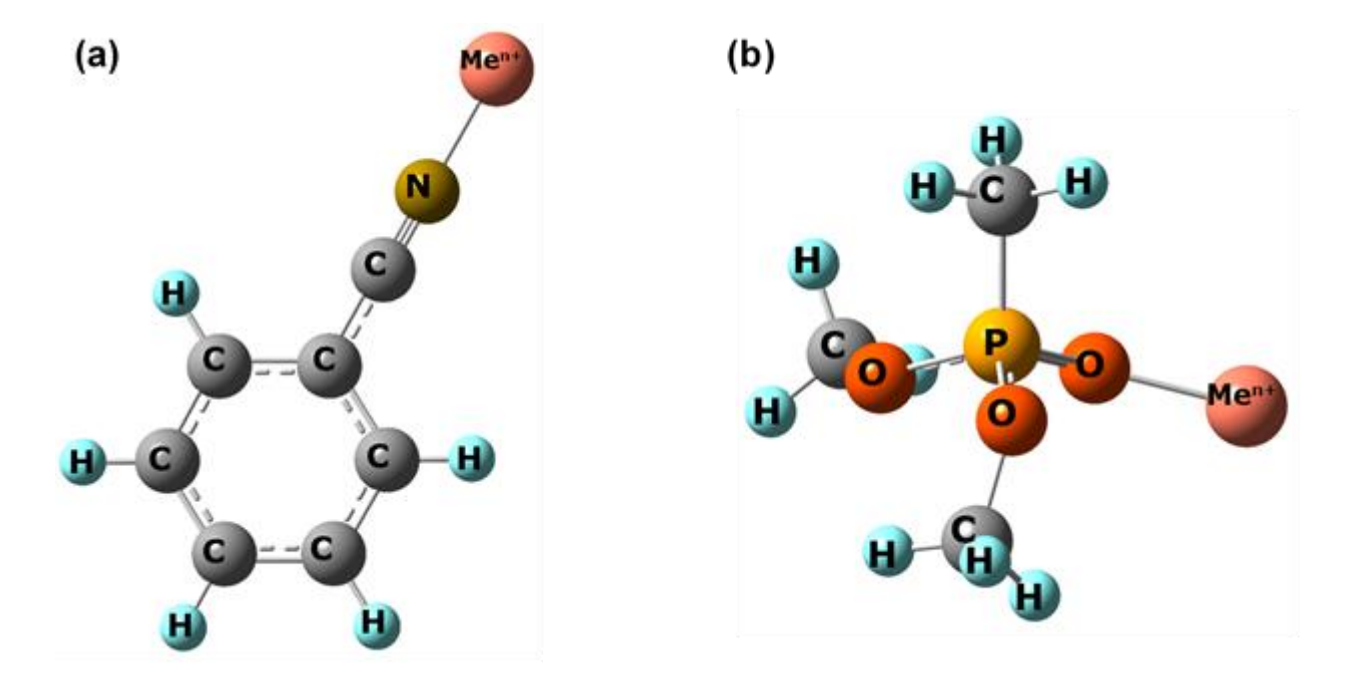


Figure 1: Representative minimum energy structures of metal cations (Meⁿ⁺) bound to (a) PhCN and (b) DMMP. Structural details for all cations studied are given in the supplementary information.

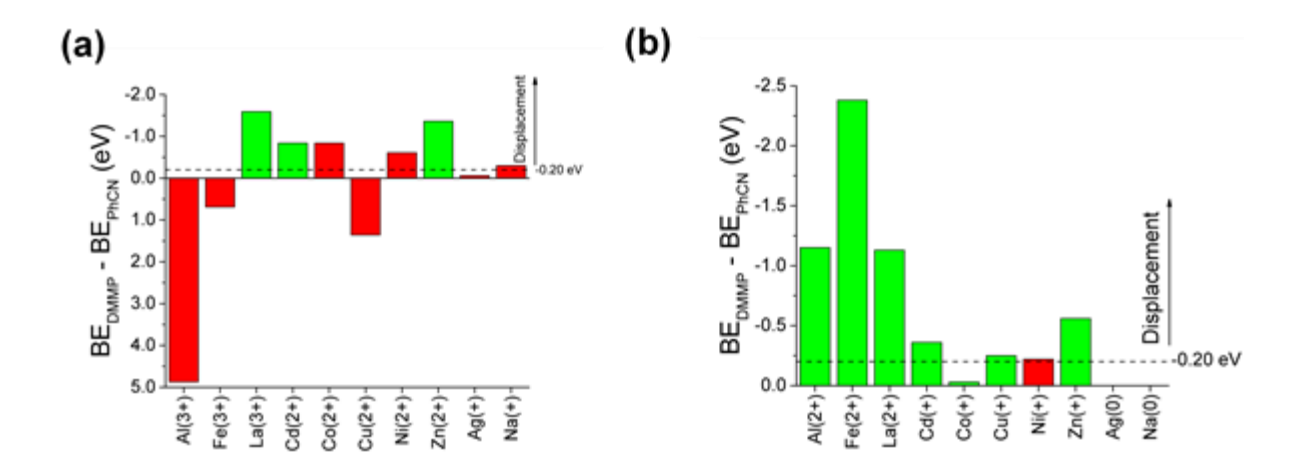


Figure 2: Calculated displacement energy ($BE_{DMMP} - BE_{PhCN}$) for displacement of PhCN by DMMP using (a) the *formal charge* approach, and (b) the *reduced charge* approach. Displacement is predicted to occur when the displacement energy is stronger (more negative) than -0.20 eV. Green bars represent agreement between theoretical predictions and experimental observations, whereas red bars show disagreement. Ag⁰ and Na⁰ are not predicted to exhibit homeotropic anchoring (in agreement with experiments), so no color bar is shown for those entries.

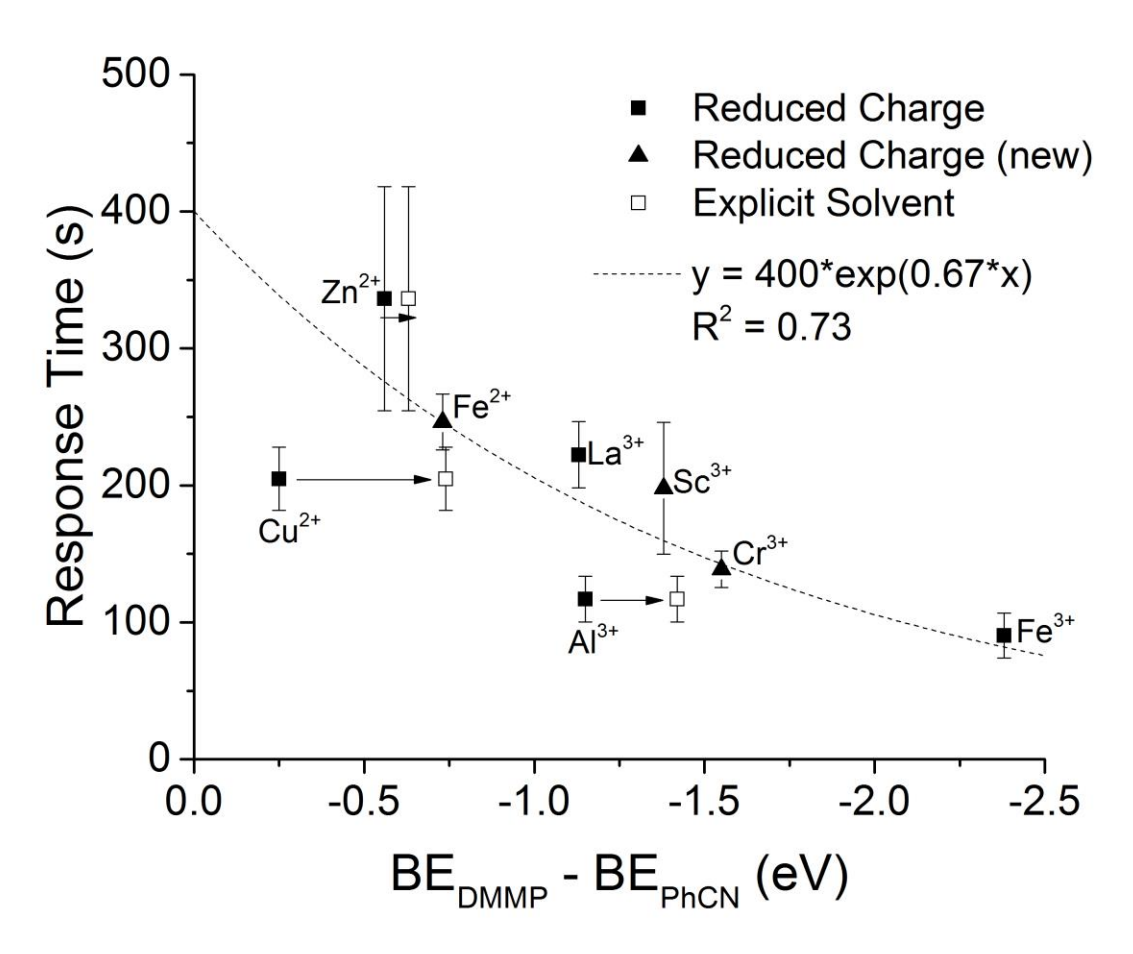


Figure 3: Response time of 5CB anchored to various metal salts to DMMP exposure as a function of calculated displacement energy. The response time was defined as the time required to reach 80% normalized light intensity. Filled squares represent values for metal cations in the original dataset of *reduced charge* calculations and corresponding experiments. The best-fit curve was calculated from these original data points, with the exception of the Cu outlier. Filled triangles represent new (Cr³⁺, Sc³⁺, Fe²⁺) cations with response times predicted by the *reduced charge* model and evaluated experimentally. The hollow data points represent data calculated from a solvent-explicit model, as described in the text. Experimental error bars are drawn one standard deviation from the mean. All charge designations shown in the figure correspond to the metal salt precursor charges from experiments.

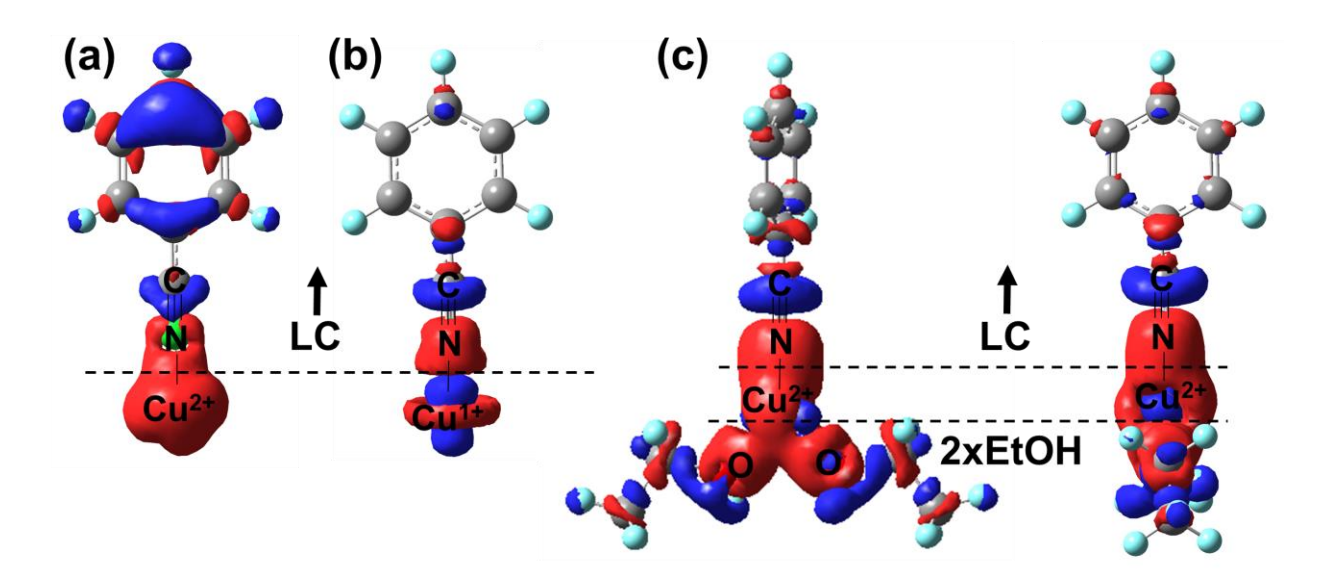


Figure 4: Calculated charge density difference plots for the interaction between a Cu cation and PhCN, using (a) the *formal charge* approach, (b) the *reduced* charge approach, and (c) the *formal charge* approach incorporating two EtOH (solvent) molecules (two views of the same complex are provided for clarity). EtOH donates electron density to Cu²⁺, lowering its effective charge. Electronic charge density depletion from the aromatic ring is significantly reduced in the presence of EtOH, as in the case of the *reduced charge* model shown in (b). Red represents electron charge accumulation and blue electron charge depletion; an isovalue of 0.005 e/ų was used to construct the surfaces.

Towards First-Principles Molecular Design of Novel Liquid Crystals-Based Chemoresponsive Systems

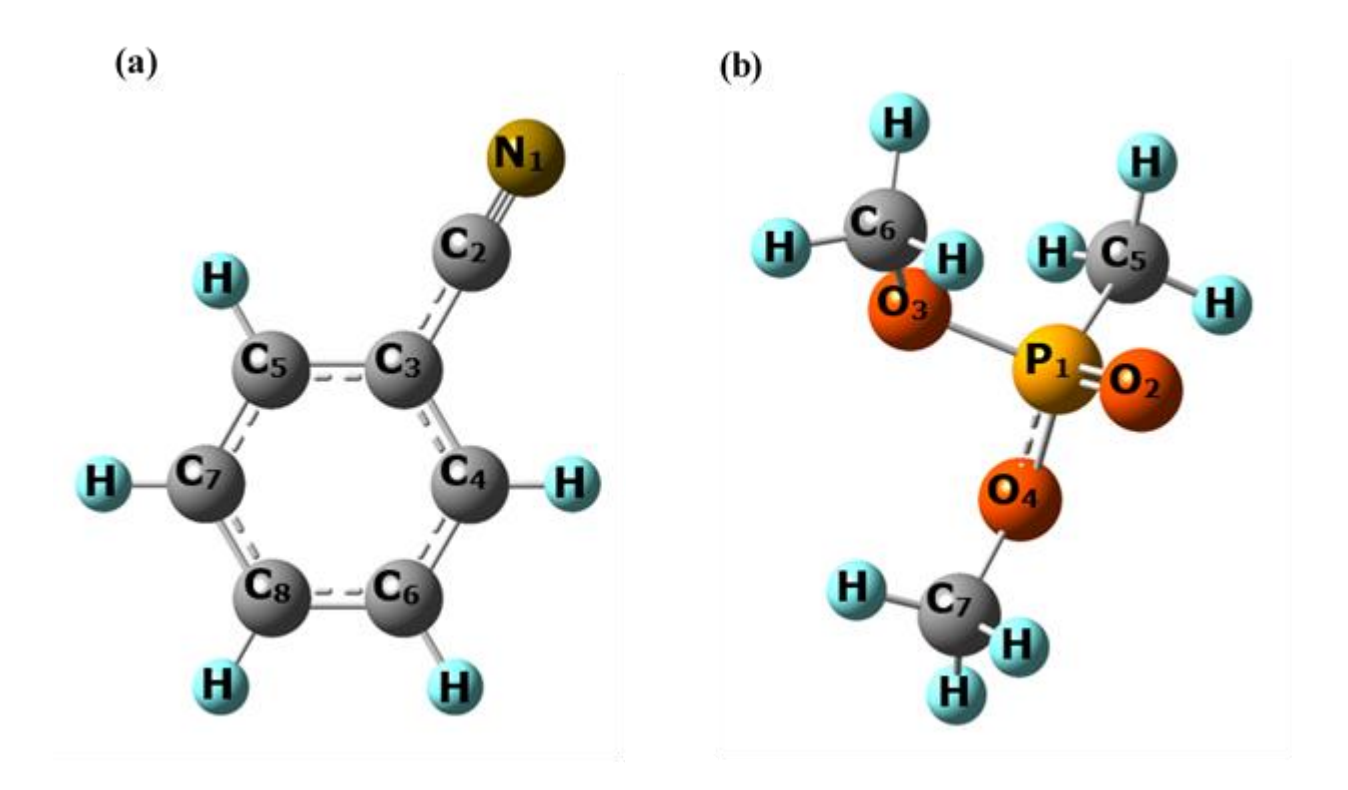
Supplementary Information

Luke T. Roling $^{\alpha}$, Jessica Scaranto $^{\alpha}$, Jeffrey A. Herron, Huaizhe Yu, Sangwook Choi, Nicholas L. Abbott, Manos Mavrikakis*

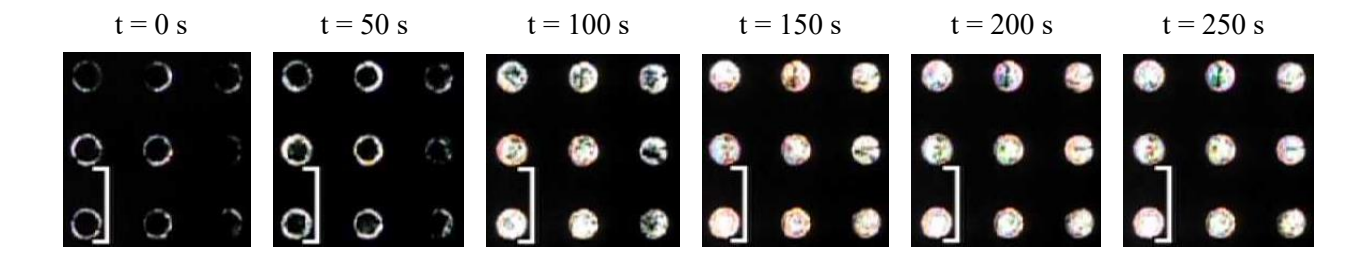
Department of Chemical and Biological Engineering, University of Wisconsin-Madison 1415 Engineering Drive, Madison, Wisconsin 53706-1607

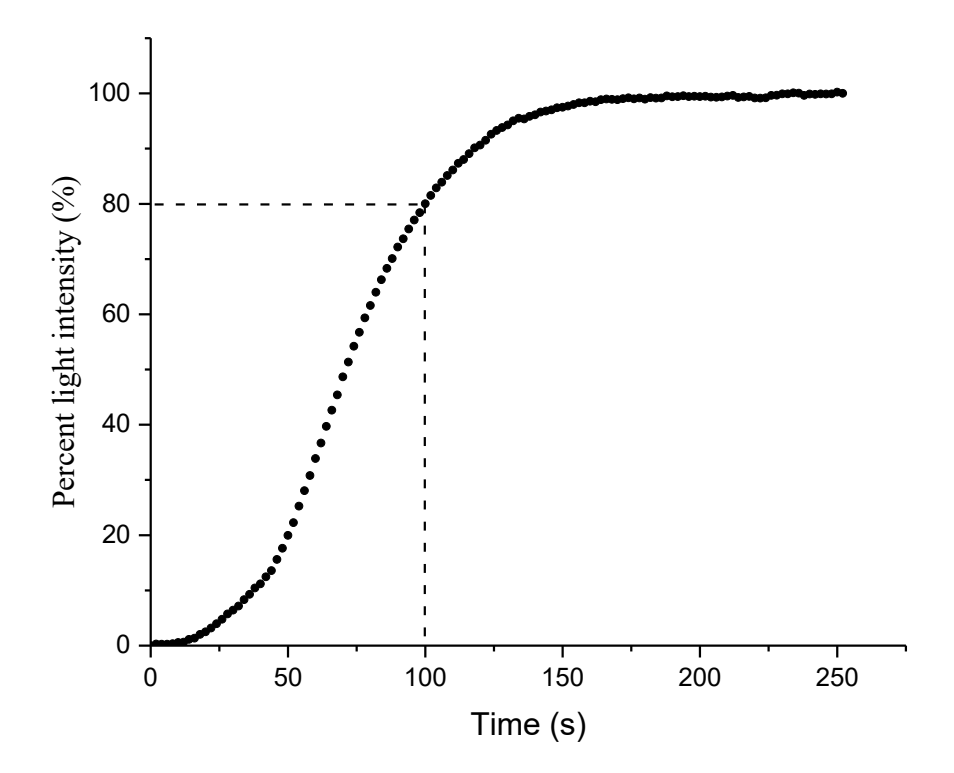
*corresponding author: emavrikakis@wisc.edu

Supplementary Figures

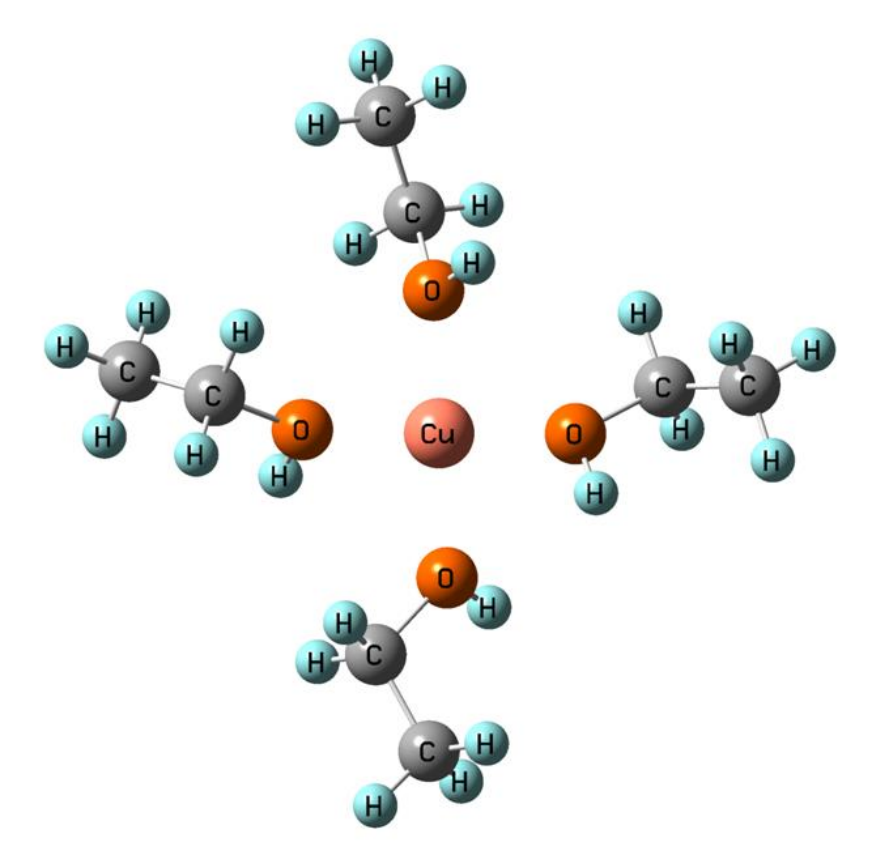


Supplementary Figure 1: Optimized structures of gas-phase (a) benzonitrile (PhCN), and (b) dimethyl methylphosphonate (DMMP). Optimized structural parameters are provided in Supplementary Table 1 for PhCN and in Supplementary Table 2 for DMMP.

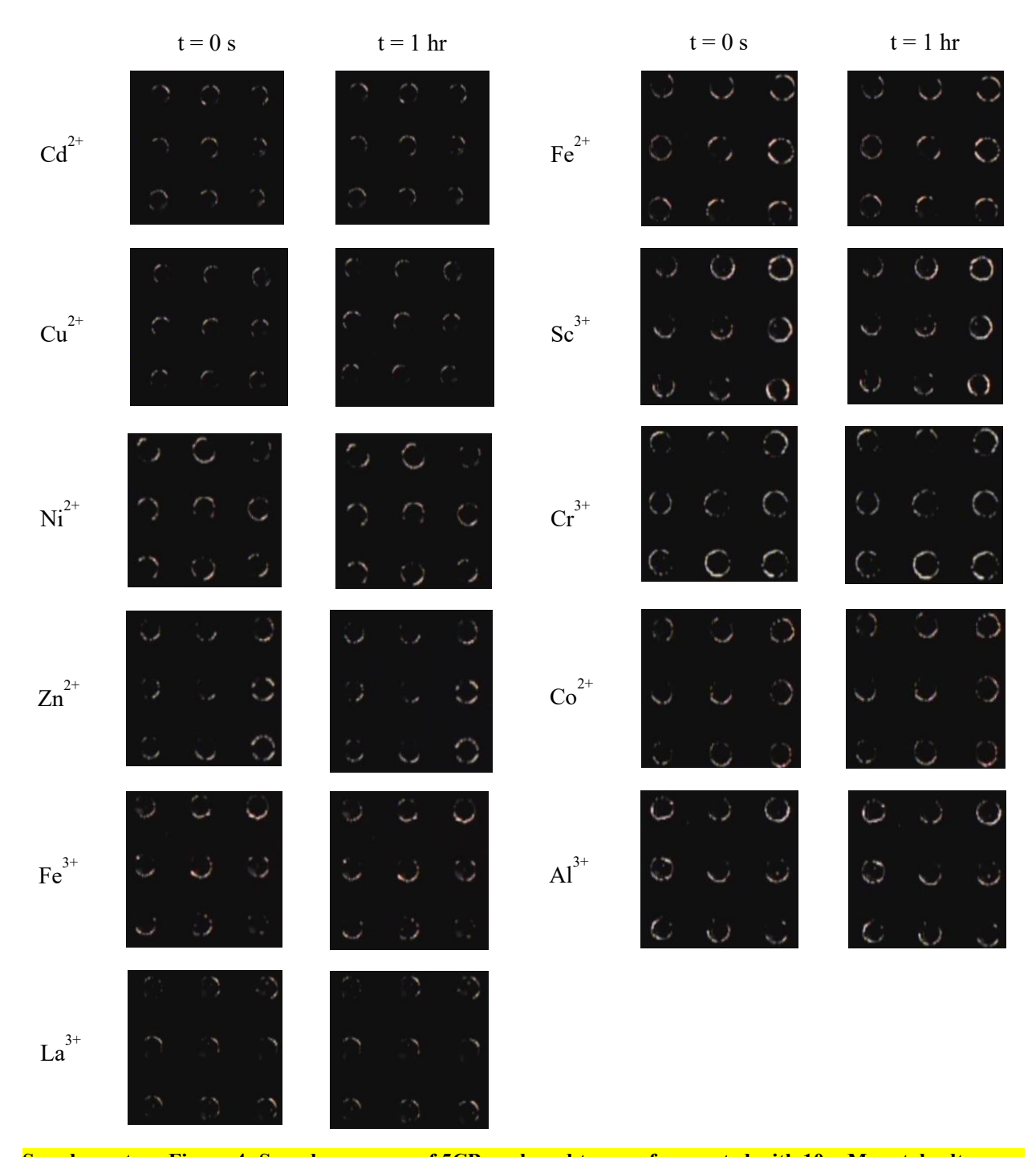




Supplementary Figure 2: Sample dynamic response of 5CB anchored to a surface coated with 10 mM Al^{3+} upon exposure to 10 ppm DMMP at t=0 s. The dotted line indicates the characteristic response time, defined as the time taken to reach 80% normalized light intensity (in this sample, 100 s).



Supplementary Figure 3: Calculated minimum energy structure of Cu^{2+} solvated by 4 ethanol (EtOH) molecules. Charge density is donated from the solvent to the cation, lowering the effective charge on the cation.



Supplementary Figure 4: Sample response of 5CB anchored to a surface coated with 10 mM metal salts upon exposure for one hour to air containing water vapor (room temperature is 26 °C and relative humidity is 31%).

Supplementary Tables

Supplementary Table 1: Main structural parameters [bond lengths in Å, angles in °] for energy-optimized gas phase benzonitrile (PhCN). Labels correspond to atoms shown in Supplementary Figure 1a. All C-H bond lengths are between 1.08-1.09 Å.

Parameter	CBS-QB3	B3LYP/CEP-121G	Experimental ¹
$N_1 - C_2$	1.16	1.19	1.16
$C_2 - C_3$	1.43	1.45	1.45
$C_3 - C_4$	1.40	1.42	1.39
$C_4 - C_6$	1.39	1.41	1.40
$C_6 - C_8$	1.39	1.42	1.40
$C_4 - C_3 - C_5$	120.0	120.1	121.6
$C_3 - C_4 - C_6$	119.7	119.7	119.0
$C_4 - C_6 - C_8$	120.2	120.2	120.1
$C_6 - C_8 - C_7$	120.1	120.1	120.1

Supplementary Table 2: Main structural parameters [bond lengths in Å, angles in °] for energy-optimized gas phase dimethyl methylphosphonate (DMMP). Labels correspond to atoms shown in Supplementary Figure 1b. All C-H bond lengths are between 1.08-1.09 Å.

Parameter	CBS-QB3	B3LYP/CEP-121G	Computed ²
$P_1 - O_2$	1.47	1.60	1.48 - 1.51
$P_1 - O_3$	1.60	1.74	1.59 - 1.63
$P_1 - O_4$	1.61	1.74	1.61 - 1.65
$P_1 - C_5$	1.80	1.86	1.79 - 1.81
$O_2 - P_1 - C_5$	116.5	121.6	116.4 - 116.8
$O_2 - P_1 - O_3$	117.3	113.4	116.4 - 117.4
$O_2-P_1-O_4$	113.4	113.4	113.3 - 113.9
$P_1-O_3-C_6$	120.0	120.4	115.5 - 119.7
$P_1-O_4-C_7$	121.3	120.4	116.1 - 120.4
$O_3 - P_1 - O_4$	101.3	105.8	100.4 - 101.7

Supplementary Table 3: Selected structural parameters calculated for the energy-optimized Me^{n+} – PhCN and Me^{n+} – DMMP systems using the *formal charge* approach.

	N	$Me^{n+}-P$	hCN	$Me^{n+}-DMMP$			
	Bond Length (Å)		Angle (°)	Bond Length (Å)		Angle (°)	
Me ⁿ⁺	$N-Me^{n^+}$	C-N	$C-N-Me^{n+}$	$O-Me^{n+}$	P – O	$P - O - Me^{n+}$	
A1 ³⁺	2.02	1.16	180.0	1.69	1.64	166.4	
Fe^{3+}	1.96	1.16	180.0	1.84	1.55	175.1	
La^{3+}	2.23	1.23	180.0	2.08	1.76	166.3	
Cd^{2+}	2.14	1.20	147.1	2.12	1.69	103.9	
Co^{2+}	1.83	1.15	180.0	1.83	1.56	101.2	
$Cu^{2^{+}}$	1.83	1.16	179.7	1.80	1.55	157.1	
Ni^{2+}	1.87	1.15	180.0	1.83	1.56	101.1	
Zn^{2+}	1.91	1.17	143.5	1.88	1.55	101.9	
Ag^+	2.13	1.18	180.0	2.13	1.64	152.4	
Na ⁺	2.24	1.16	180.0	2.09	1.50	168.5	

Calculated parameters for isolated molecules are 1.16 Å (C – N) and 1.47 Å (P – O).

Supplementary Table 4: Selected structural parameters calculated for the energy-optimized Me^{n+} – PhCN and Me^{n+} – DMMP systems using the *reduced charge* approach.

	N	$\sqrt{1}e^{n^+} - P$	hCN	$Me^{n+}-DMMP$		
	Bond Length (Å)		Angle (°)	Bond Length (Å)		Angle (°)
Me ⁽ⁿ⁻¹⁾⁺	$N-Me^{n^+}$	C-N	$C-N-Me^{n+}$	$O-Me^{n+}$	P – O	$P - O - Me^{n+}$
Al ²⁺	2.66	1.15	180.0	1.67	1.61	157.6
Fe^{2+}	1.94	1.16	180.0	1.77	1.58	151.3
La^{2+}	2.39	1.20	180.0	2.18	1.69	172.3
Cd^+	2.25	1.19	180.0	2.15	1.64	162.6
Co^+	1.83	1.16	180.0	1.86	1.52	147.4
Cu^+	1.81	1.16	180.0	1.83	1.51	142.3
Ni^+	1.82	1.16	180.0	1.84	1.52	143.4
Zn^+	2.02	1.16	180.0	1.93	1.51	157.4
Ag^0	2.51	1.19	137.4	2.45	1.62	147.6
Na ⁰	2.37	1.16	147.4	2.23	1.48	172.9

Calculated parameters for isolated molecules are 1.16 Å (C – N) and 1.47 Å (P – O).

Supplementary Table 5: Comparison of water binding energies to metal cations with the respective binding energies of PhCN and DMMP using the *reduced charge* approach (all charges listed are reduced charges). The italicized entries correspond to those systems for which homeotropic anchoring is not observed experimentally. All values are in eV.

-			BE(H ₂ O)		BE(H ₂ O)
Cation	$BE(H_2O)$	BE(PhCN)	- BE(PhCN)	BE(DMMP)	- BE(DMMP)
Al^{2+}	-4.25	-7.45	3.20	-8.60	4.35
Cr^{2+}	-3.14	-5.62	2.48	-7.17	4.03
$\mathrm{Fe^{2+}}$	-3.57	-5.70	2.13	-8.08	4.51
La^{2+}	-2.66	-4.06	1.40	-5.19	2.53
Sc^{2+}	-2.63	-4.09	1.46	-5.47	2.84
Cd^+	-1.44	-1.91	0.47	-2.27	0.83
Co^+	-1.53	-2.51	0.98	-2.54	1.01
Cu^+	-1.62	-2.56	0.94	-2.81	1.19
Fe^+	-1.33	-2.27	0.94	-3.00	1.67
Ni^+	-1.67	-2.56	0.89	-2.78	1.11
Zn^+	-1.44	-2.23	0.79	-2.79	1.35
Ag^0	-0.13	-0.08	-0.05	-0.17	0.04
Na^0	-0.21	-0.19	-0.02	-0.44	0.22

Supplementary Discussion

Energy Minimization of DMMP and PhCN

Supplementary Figure 1 shows the energy-optimized structure of the individual gas-phase PhCN and DMMP molecules, as determined by our electronic structure calculations. Supplementary Table 1 summarizes the main structural parameters of PhCN, along with the respective experimental values¹. The structural parameters for DMMP are shown in Supplementary Table 2 alongside previously computed values² at different levels of theory; to the best of our knowledge, no experimental values for DMMP structural parameters are available. All C – H bond lengths are between 1.08 and 1.09 Å for both molecules. In general, the parameters computed at the CBS-QB3 level of theory agree with the experimental or previously computed parameters better than those at the B3LYP/CEP-121G level of theory.

Energy Minimization of DMMP and PhCN Complexes with Metal Cations

Supplementary Table 3 shows the main structural parameters of the Meⁿ⁺-PhCN and Meⁿ⁺-DMMP complexes with the *formal charge* approach, and Supplementary Table 4 shows the main structural parameters of those complexes with the *reduced charge* approach. The interaction of metal cations with the PhCN molecule only slightly affects the C–N bond length (1.16 Å with CBS-QB3 for isolated PhCN), with the exception of PhCN–La³⁺ (1.23 Å), while the interaction between Meⁿ⁺ and DMMP generally leads to an increased P–O bond length (1.47 Å for isolated DMMP). The C–N–Meⁿ⁺ bond angle is 180° (i.e. linear), except for the cases of Zn²⁺, Cd²⁺, Ag⁰ and Na⁰, in which slight bending occurs. No particular trend is observed for the P–O –Meⁿ⁺ bond angle. The N–Meⁿ⁺ bond length is generally longer than the O–Meⁿ⁺ bond length.

Correlation of Response Time with Calculated Binding Energies

An exponential curve relating the experimental response time to the calculated binding energies was chosen for fundamental reasons underlying the displacement of the liquid crystal from the surface. In particular, we can understand the experimental response time in the context of reaction rates; specifically, the inverse of the response time corresponds to the reaction rate. Assuming an Arrhenius-type expression for reaction rates, we can write:

$$\frac{1}{response\ time} \propto rate = \left(\prod_{i} [C_i]\right) * A * \exp(\frac{-E_A}{RT})$$

where $[C_i]$ are the respective concentration terms, A is the pre-exponential term, E_A is the activation energy, R is the gas constant, and T is the absolute temperature. In the context of this displacement reaction, we assume that $[C_i]$ and A are invariant when changing metal cations, so the response time is determined directly by the exponential term. Assuming that there exists a Brønsted-Evans-Polanyi correlation^{3,4} between the activation energy of the displacement event (E_A) and the reaction free energy (ΔG) , this allows approximation of activation energies as a linear function of the reaction energy; i.e., $E_A = \alpha * (\Delta G) + \beta$, for some parameters α and β . Since ΔG for this displacement is dominated by the difference in binding energies (i.e. $BE_{DMMP} - BE_{PhCN}$) due to consistent entropic effects, E_A can be replaced in the exponential by the difference in binding energies. The parameter β can be pulled into a modified pre-exponential term along with the constant concentration terms, and the entire expression inverted to yield the final expressions for response time as given in our model.

$$\frac{1}{response\ time} \propto \left(\prod_{i} [C_i] \right) * A * \exp\left(\frac{-\alpha (BE_{DMMP} - BE_{PhCN}) + \beta}{RT} \right)$$

response time
$$\propto A' * \exp(\frac{\alpha(BE_{DMMP} - BE_{PhCN})}{RT})$$

In this sense, our exponential fit provides us the values of α and A' corresponding to this reaction event. We note that exact determination of the terms contained in A' would require more experiments outside the scope of this work.

According to this convention, our linear fit predicts finite response times at $\Delta BE = 0$. This is a physically reasonable result, since even positive (unfavorable) differences in binding energy could still result displacement events if the concentration of DMMP is sufficiently high to overcome an unfavorable reaction equilibrium constant. Our model is developed in the experimental context of 10 ppm DMMP. Accurately accounting for the effect of changing this concentration is outside the scope of this work, due to complications including possible mass transfer limitations.

Charge Transfer from Ethanol Solvent

We hypothesize that some residual ethanol (EtOH) molecules from experimental preparation of the substrate surface containing the metal cations might remain bound to the metal cation as a possible consequence of a strong interaction between the cation and EtOH in solution, and that the charge of the solvated metal cation is therefore different from its *formal charge* due to donation of electron density from the EtOH solvent to the cation. To test this hypothesis, we calculated the differential binding energy (BE_{diff}) and optimized cation charge (q_f) resulting from the relaxation of a Cu²⁺ cation (formal charge) in the presence of n EtOH molecules (n = 1 - 4). BE_{diff} for the nth EtOH molecule is defined as follows:

 $BE_{\text{diff}} = E_{\text{Me+}n\text{EtOH}} - E_{\text{Me+}(n-1)\text{EtOH}} - E_{\text{EtOH}}$

where $E_{\text{Me+}n\text{EtOH}}$ and $E_{\text{Me+}(n\text{-}1)\text{EtOH}}$ are the total energies of the complex with n and (n-1) EtOH molecules, respectively, and E_{EtOH} is the total energy of the isolated EtOH molecule.

The optimized structure of $[Cu(EtOH)_4]^{2^+}$ is shown in Supplementary Figure 6. All O – Cu distances in $[Cu(EtOH)_4]^{2^+}$ are calculated to be between 1.95-1.96 Å, which agree with the experimental value of 1.97 Å reported by Inada et al. for the solvation of Cu(II) by an average of four EtOH molecules⁵. We find that q_f decreases to 1.47, 0.68, 0.59, 0.31 as n increases from 1 to 4, respectively. These data suggest that the solvated Cu cation has a q_f smaller than (2+) and its value is closer to the charge used in the *reduced charge* approach, particularly when the Cu cation interacts with 1-2 EtOH molecules (q_f is a strong function of n). BE_{diff} also decreases to -6.1 eV, -4.6 eV, -2.2 eV, -1.9 eV as n increases from 1 to 4, respectively, which qualitatively follows our observation that cations in the *reduced charge* model bind species more weakly than those in the *formal charge* model. The decrease of the metal charge as function of the number of EtOH molecules in the complex is in agreement with related computational studies of metal cation solvation by Rao et al. ⁶ and by Xu et al. ⁷.

In order to further investigate this phenomenon, we computed BE_{PhCN} and BE_{DMMP} to Cu^{2+} in the presence of one and two EtOH molecules. In the presence of one EtOH molecule, we calculated $BE_{PhCN} = -6.08$ eV and $BE_{DMMP} = -4.86$ eV. In this case, the BEs are between the values obtained using the *reduced charge* approach (-2.56, -2.81) and those obtained with the *formal charge* approach (-9.88, -8.52). Importantly, since PhCN binds more strongly than DMMP in this calculation, the model predicts that displacement of PhCN by DMMP will not occur, in contrast to experimental results. We performed the same calculations in the presence of two EtOH molecules, obtaining $BE_{PhCN} = -2.99$ eV and $BE_{DMMP} = -3.73$ eV, which would predict displacement of PhCN by DMMP, in agreement with experiments. These two values are within 1

eV of the values calculated with the *reduced charge* approach, demonstrating reasonable qualitative agreement between this larger system containing Cu²⁺ bound to two EtOH molecules and the *reduced charge* model.

Effect of Charge Donation from Chemical Species in the Sensing Surface Environment

In addition to the ethanol solvent, other species may contribute to the donation of charge density to metal cations, thereby reducing their charge from the formal charge in the metal salt precursor. As a brief example, water is omnipresent in the environment of our experiments and can also donate charge through coordination with the metal cation through one of its lone electron pairs. However, we calculate that a metal cation interacts with water substantially more weakly than with ethanol. For example, a single water molecule binds to Cu²⁺ with an energy of -4.56 eV, which is weaker than the binding of both the first (-6.1 eV) and second (-4.6 eV) EtOH molecules described earlier. Further, the binding energy of water to Cu¹⁺ (reduced charge) is just -1.60 eV, so once Cu²⁺ is reduced in the presence of two EtOH molecules, adsorption of a third and fourth EtOH molecule would still be preferable to adsorption of water. The metal cation will therefore strongly prefer to maintain coordination to any trace EtOH remaining from synthesis of the salt surface rather than coordinate to free water molecules, justifying our selection of EtOH as the charge-donating species in our model.

Supplementary References

- Hellwege, K. H. A. M. Landolt-Bornstein: Group II: Atomic and Molecular Physics Volume 7: Structure Data of Free Polyatomic Molecules. (Springer-Verlag, 1976).
- Yang, L., Shroll, R. M., Zhang, J. X., Lourderaj, U. & Hase, W. L. Theoretical Investigation of Mechanisms for the Gas-Phase Unimolecular Decomposition of DMMP. *J. Phys. Chem. A* **113**, 13762-13771 (2009).
- Evans, M. G. & Polanyi, M. Inertia and driving force of chemical reactions. *Transactions of the Faraday Society* **34**, 11-24 (1938).

- 4 Bell, R. P. The Theory of Reactions Involving Proton Transfers. *Proceedings of the Royal Society of London. Series A Mathematical and Physical Sciences* **154**, 414-429 (1936).
- Inada, Y., Hayashi, H., Sugimoto, K. & Funahashi, S. Solvation structures of Manganese(II), iron(II), cobalt(II), nickel(II), copper(II), zinc(II), and gallium(III) ions in methanol, ethanol, dimethyl sulfoxide, and trimethyl phosphate as studied by EXAFS and electronic spectroscopies. *J. Phys. Chem. A* **103**, 1401-1406 (1999).
- Rao, J. S., Dinadayalane, T. C., Leszczynski, J. & Sastry, G. N. Comprehensive Study on the Solvation of Mono- and Divalent Metal Cations: Li+, Na+, K+ Be2+, Mg2+ and Ca2+. *J. Phys. Chem. A* **112**, 12944-12953 (2008).
- Xu, M. J., Dou, X. M., Bu, Y. X. & Zhang, Y. F. Density functional theory calculations for the microsolvation of M3+-zwitterionic glycine complexes (M3+ = Al3+, Ga3+, In3+). *Chem. Phys. Lett.* **537**, 101-106 (2012).